

FENET: FOCUSING ENHANCED NETWORK FOR LANE DETECTION

Liman Wang*, Hanyang Zhong*

University of York;
{lw2391, hanyang.zhong}@york.ac.uk

ABSTRACT

Inspired by human driving focus, this research pioneers networks augmented with Focusing Sampling, Partial Field of View Evaluation, Enhanced FPN architecture and Directional IoU Loss - targeted innovations addressing obstacles to precise lane detection for autonomous driving. Experiments demonstrate our Focusing Sampling strategy, emphasizing vital distant details unlike uniform approaches, significantly boosts both benchmark and practical curved/distant lane recognition accuracy essential for safety. While FENetV1 achieves state-of-the-art conventional metric performance via enhancements isolating perspective-aware contexts mimicking driver vision, FENetV2 proves most reliable on the proposed Partial Field analysis. Hence we specifically recommend V2 for practical lane navigation despite fractional degradation on standard entire-image measures. Future directions include collecting on-road data and integrating complementary dual frameworks to further breakthroughs guided by human perception principles. Code will be made available.

Index Terms— Lane Detection, Neural Networks, Focusing, Sampling, Self-driving

1. INTRODUCTION

The present study delineates the disparity between human visual focus during driving and the perspectives captured by 2D cameras. Fig. 1 illustrates that experienced drivers preferentially gaze at distant road regions, a strategy crucial for anticipating path geometry and steering adjustments [1, 2, 3]. This behaviour, particularly evident around curves, involves gazing 1-2 seconds ahead into critical preview zones [2, 4]. Inspired by these human focus patterns, our research introduces the 'Focusing Sampling' method, aimed at enhancing the detection and regression of distant lane boundary markings, a key challenge in high-speed autonomous driving. Additionally, 'Partial Field of View Evaluation' is proposed to improve accuracy assessments in real-world scenarios, emphasizing the forward road sections align with driver focus.

In the realm of lane detection, prevalent models such as CLRNNet [5] and GANet [6] rely on uniform multi-scale fea-

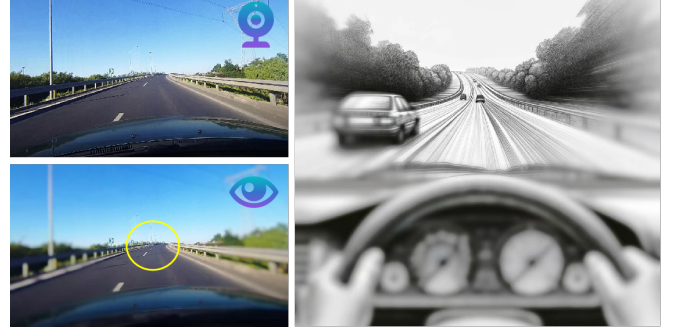


Fig. 1. Skilled drivers focus their gaze far ahead on the road. The upper left image shows the **full camera view**, while the lower left image visualizes where **experienced drivers look** - far ahead along the road and lane lines.

ture pyramid network (FPN) architectures. These models, however, do not adequately capture the global spatial context, essential for detailing key road aspects for safe navigation. Even though transformers are known for their global semantic processing capabilities [7], their efficiency diminishes when identifying slender, elongated lane markings, where cardinal cues are sparse. Lane boundaries also display substantial scale variations and are affected by diverse lighting and surface conditions [8]. To overcome these challenges, our study introduces either positional or standard non-local blocks into the FPN, enriching it with extensive global context information. Furthermore, subsequent experiments demonstrate that 'Directional IoU Loss' not only matches but can even exceed the benefits offered by positional non-local blocks.

This research contributes four innovations: (1) 'Focusing Sampling,' a training strategy prioritizing small and distant lane details; (2) 'Partial Field of View Evaluation,' new metrics for accuracy in forward road sections critical for real-world applications; (3) an enhanced FPN architecture that incorporates either positional non-local blocks or standard non-local blocks, depending on the requirement; (4) 'Directional IoU Loss,' a novel regression loss that addresses directional discrepancies in distant lanes. FENetV1, employing positional non-local blocks, achieves state-of-the-art results on conventional metrics by concentrating on perspective-dependent semantics. On the other hand, FENetV2, which in-

* Co-first author

* Co-first author

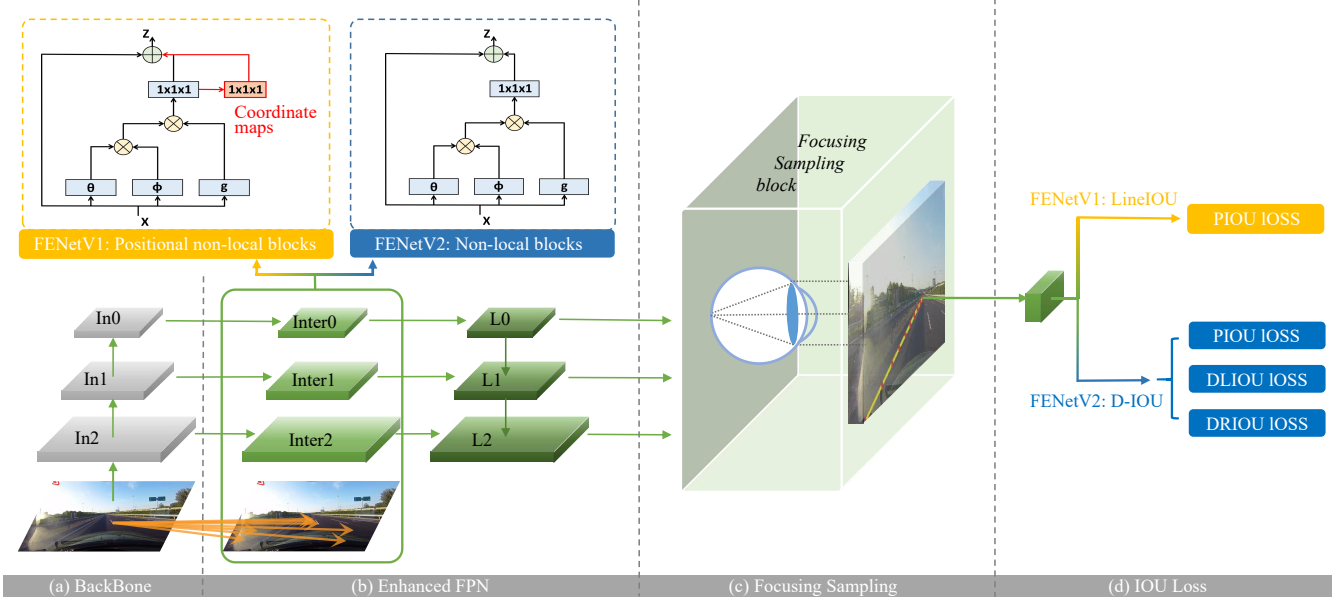


Fig. 2. Architecture of the FENet lane detection framework, which uses a DLA34 backbone and Enhanced FPN. The input layers feed into internal layers integrated with **positional non-local blocks** (for FENetV1 or standard non-local blocks (for FENetV2) to capture spatial context. The internal layers connect to output layers that pass through **Focusing Sampling** and either standard IOU loss (for FENetV1) or **Directional IOU loss** (for FENetV2). FENetV1 (yellow pathway) and FENetV2 (blue pathway) share the common green pathway, with distinct supplementary modules.

tegrates coordinate modelling into the 'Directional IoU Loss', excels in boundary localization accuracy for distant lanes. Although FENetV2 may underperform slightly in conventional metrics compared to FENetV1, its specialization in distant lane regression makes it more suited for practical navigation. In essence, this pioneering work advocates for the enhancement of regression-focused models and evaluations, employing targeted techniques that prioritize the representation and assessment of road details vital for accurate and safe autonomous lane detection.

2. RELATED WORKS

Deep learning-based lane prediction methods can be categorized into semantic segmentation, anchor-based, and parameter-based approaches. Semantic segmentation methods like SCNN [9], SAD [10], and Curvelanes-NAS [11] use pixel-level predictions for accuracy but have high computational complexity. Anchor-based methods like CLR-Net [5], GANet [6], E2E-LMD [12], IntRA-KD [13], UFLD/UFLDV2 [14, 15], CondLaneNet [16], and LaneATT [17] are fast but less accurate in complex scenarios. Parameter-based methods like "Efficient Lane Detection via Curve Modeling" [18] use curve anchors for efficiency but lack optimal accuracy. We build on prior work to address limitations in accuracy and complexity.

3. METHODOLOGY

3.1. Focusing Sampling

Motivation. Existing uniform point sampling strategies fail to properly weigh the visual perspective critical to robust lane detection. These methods treat all image regions equally, despite lanes containing more valuable semantic information at distant vanishing points, especially along curves [19]. To address the resulting deficiencies in understanding upcoming lanes, we propose a Focusing Sampling technique inspired by adept drivers' visual attention directed far down the road. Like drivers who gaze ahead to foresee curves [1], Focusing Sampling emphasizes distant details while still examining nearby points. As demonstrated in Fig. 3, this novel approach properly accounts for complete lane geometry and handles complex turn and curve cases. Focusing Sampling is targeted to transform limitations of uniform sampling that risk losing data and semantics critical to lane prediction.

Formulation. Building on the foundation of uniform sampling, we propose using a logarithmic-based Focusing Sampling, for which an intuitive comparison is made in Fig. 8 in Appendix A.1. The formula for this Focusing Sampling is:

$$y = \frac{H}{N_{sample} - 1} * \log_{feature} a_n \quad (1)$$

where $a_n = \frac{1}{N_{sample}-1} * i$. $feature$ is the feature point number in the network. To produce focusing sample

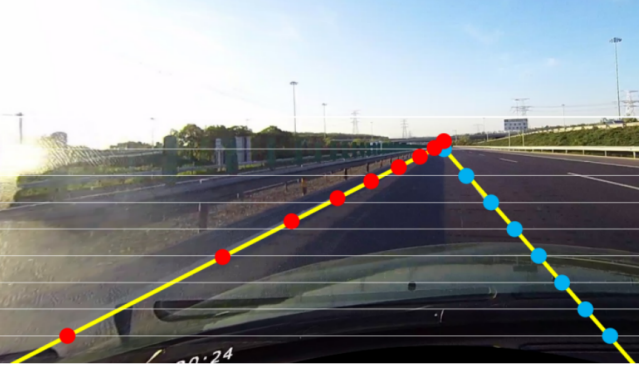


Fig. 3. Visual depiction comparing **Focusing Sampling** (red dots) versus **uniform sampling** (blue dots). Focusing Sampling strategically emphasizes critical distant vanishing points along the lane while retaining informative nearby points. This accounts for perspective geometry, unlike standard uniform sampling that weights all regions equally.

points in this range, a logarithmic transformation is applied to the feature distribution, mapping the original feature points to integer sample points. H denotes the image height and N_{sample} is the number of sampling points, while a_n represents an arithmetic sequence generated within the range of 0 to 1 across i data points. This logarithmic approach selects valuable semantic information. As an application of the logarithmic discretization introduces the possibility of repeated integer values, post-processing includes deduplication of the sample points. Complete details on the feature discretization process and resulting distribution are provided visually in the code and Appendix Fig. 8.

3.2. Positional Non-local Block and Position Enhanced FPN structure

Motivation. CLRNNet principally employs the Feature Pyramid Network (FPN) architecture for lane detection [5]. While excelling at multi-scale feature extraction, FPN possesses certain limitations. Specifically, deeper network layers emphasize semantic representations, whereas shallow layers prioritize fine-grained details, culminating in suboptimal detection of diminutive targets. To augment FPN, we introduce a structure assimilating non-local blocks [20], inspired by enhancements in PANet and Mask R-CNN [21, 22]. This approach injects contextual clues into the network while preserving its depth and enhancing its multi-scale properties. Moreover, based on the distinctiveness of lane marking objectives, we propose a Position Enhanced FPN (PEFPN) module to actualize tighter integration between global semantics and lane coordinate modelling. As delineated in Fig. 2 Positional non-local blocks, and expanded upon Fig. 7 in Appendix A.1, position information is directly infused into multi-scale feature maps within the Enhanced FPN.

Formulation. The coordinate map equations utilize spatial indices i and j to index each pixel location in the feature map, where i iterates vertically over the height dimension H , and j iterates horizontally over the width dimension W . Specifically, i ranges from 1 to H , indexing each row, while j ranges from 1 to W . The x-coordinate map is calculated as follows:

$$x_{coord}(i, j) = \frac{2(j-1)}{W-1} - 1, \text{ for } i = 1 \dots H, j = 1 \dots W \quad (2)$$

Similarly, the y-coordinate map is:

$$y_{coord}(i, j) = \frac{2(i-1)}{H-1} - 1, \text{ for } i = 1 \dots H, j = 1 \dots W \quad (3)$$

This positional non-local block provides an enriched set of features encoding both global contexts as well as precise spatial locations. Furthermore, we apply the proposed Focusing Sampling technique on top of this architecture to selectively concentrate on lane segments during feature extraction. The samples provide strong cues to track lane coordinates and directionality. The FENetV1 incorporates PEFPN and Focusing Sampling that unifies refined coordinate modelling through direct coordinate injection with Focusing Sampling guided by lane positions. The ablation experiment in Appendix A.1 shows that the PEFPN represents a unique architecture designed according to the Focusing perspective for lane detection introduced in FENetV1.

3.3. Focusing Enhanced Network

Motivation. Within FENetV1, the formulation of PEFPN hinges upon the consolidated design of positional non-local blocks and Enhanced FPN architecture. Capitalizing on the distinctiveness of lane detection objectives, positional non-local blocks are devised based on coordinate map information, furnishing efficacious feature extraction. However, ablation experiments (elaborated in Appendix A.1) reveal that in the absence of Focusing Sampling, employing standard non-local blocks rather than positional non-local blocks conferred analogous performance. This validates that orientational clues from lane coordinates need not necessarily be injected at non-local locations. Therefore, guided by improving network efficiency, we conceived FENetV2 to further investigate Focusing Enhanced FPN (FEFPN) with standard non-local blocks and Directional IoU. Hence in devising FENetV2, we explore more efficient alternatives through standard non-local blocks, focusing enhancement modules, and Directional IoU formulations to preserve efficacy while enhancing computational thrift.

FEFPN Structure. As shown in Fig. 2, most architecture configurations exhibit substantial similarities with PEFPN, with the distinction that standard non-local blocks are used during the construction of internal layers (Inter0, Inter1, Inter2).

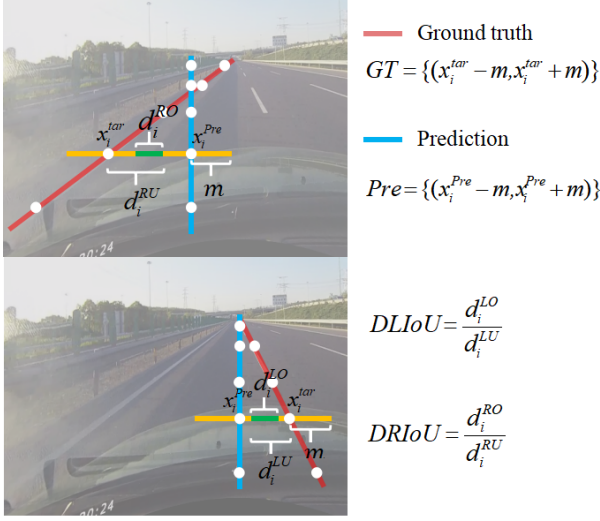


Fig. 4. D-IoU Loss. D-IoU loss evaluates model lane prediction accuracy by comparing ground truth lanes to predicted lanes. It integrates the IoU between extended lane segments from sampled points x_i along the lane. This provides a directional, localized loss metric accounting for prediction precision over the full lane geometry.

3.4. Lane Directional Intersection over Union (D-IoU) Module

Motivation. LineIoU only considers distance without directional relation [5]. Our D-IoU module, Fig. 4, ascertains directional discrepancies to improve accuracy.

Formulation. As depicted, D-IoU comprises Position-IoU (P_{IoU}), Direction Left IoU (DL_{IoU}) and Direction Right IoU (DR_{IoU}). P_{IoU} is the LineIoU module in the CLNet. DL_{IoU} and DR_{IoU} represent the Distance-IoU to the Left and Right of the ground truth points, respectively. $DLIoU_i$ is:

$$DLIoU_i = \frac{d_i^{LO}}{d_i^{LU}} = \frac{x_i^{tar} - \max(x_i^{pre} - m, x_i^{tar} - m)}{m} \quad (4)$$

m designates the pixel expansion amount for each point. After expanding by m pixels, $x_i^{pre} - m$ and $x_i^{pre} + m$ give the predicted point's left and right coordinates, respectively. The $DRIoU_i$ is a mirror mapping of the $DLIoU_i$, with similar definitions and will not be repeated.

D-IoU combines these using coefficients α, β, γ :

$$D - IoU = \alpha(1 - P_{IoU}) + \beta(1 - DL_{IoU}) + \gamma(1 - DR_{IoU}) \quad (5)$$

This provides distance and directional accuracy for precise lane alignment.

3.5. Training and Inference Details

Training Loss. The total training loss in FENetV1 is a weighted combination of several loss components:

$$L_{totalv1} = \omega_{Piou} L_{Piou} + \omega_{cls} L_{cls} + \omega_{xytl} L_{xytl} + \omega_{se} L_{se} \quad (6)$$

L_{Piou} is the PIoU Loss, weighted by ω_{Piou} , which aligns predictions with ground truth position. L_{cls} is the focal loss for classification. L_{xytl} represents regression loss for predicting start point, angle, and lane length. L_{se} is the semantic segmentation loss. The weights ω balance the contributions of each component. The training loss in FENetV2 is:

$$L_{totalv2} = \omega_{Diou} L_{Diou} + \omega_{cls} L_{cls} + \omega_{xytl} L_{xytl} + \omega_{se} L_{se} \quad (7)$$

Where L_{Diou} is the D-IoU Loss, weighted by ω_{Diou} , which aligns predictions with ground truth position and direction.

Inference. To produce the final lane detection results, we apply non-maximum suppression (NMS) to remove overlapping predictions, leaving only optimal lanes [17]. We also evaluate an NMS-free approach by setting top-k to 1 during one-to-one assignments. These refinements extract the most accurate lanes.

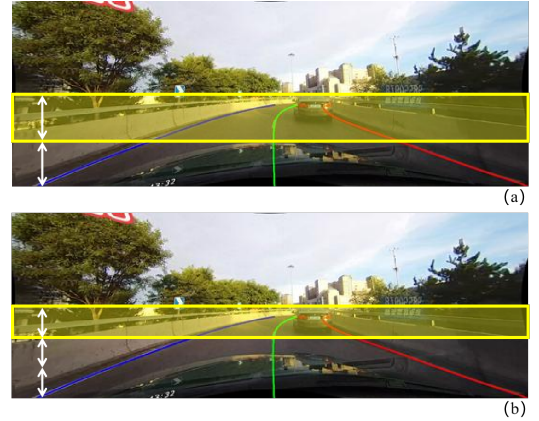


Fig. 5. The proposed **Partial Field of View** metric enhances evaluation by subdividing the lower image half into distal fraction views after preprocessing cropping. Assessing model precision on the (a) top 1/2 field and (b) top 1/3 field aligns with driving gaze ahead needs. This practical metric gauges lane detection aptitude beyond existing methods.

3.6. Augmenting Evaluation via Partial Field of View

Existing evaluation metrics for lane detection models exhibit critical limitations aligning with real-world driving needs. Metrics like pixel-wise accuracy and standard mAP treat all pixels in lane marking predictions equally, despite significant differences in their actual safety impact. However, as noted previously, experienced drivers preferentially gaze at distant road regions, a strategy crucial for anticipating path geometry

Method	Backbone	mF1	F1@50	F1@75	GFlops
UFLDV2	ResNet18	-	75	-	-
UFLDV2	ResNet34	-	76	-	-
FOLOLane	ERFNet	-	78.8	-	-
LaneAF	ERFNet	48.6	75.63	54.53	22.2
LaneAF	DLA34	50.42	77.41	56.79	23.6
LaneATT	ResNet18	47.35	75.13	51.29	9.3
LaneATT	ResNet34	49.57	76.68	54.34	18
LaneATT	ResNet122	51.48	77.02	57.5	70.5
GANet-S	ResNet18	-	78.79	-	-
GANet-M	ResNet34	-	79.39	-	-
GANet-L	ResNet101	-	79.63	-	-
CLRnet	ResNet18	55.23	79.58	62.21	11.9
CLRnet	ResNet34	55.14	79.73	62.11	21.5
CLRnet	ResNet101	55.55	80.13	62.96	42.9
CLRnet	DLA34	55.64	80.47	62.78	18.5
FENetV1(Ours)	DLA34	56.27	80.15	63.66	19.05
FENetV2(Ours)	DLA34	56.17	80.19	63.50	18.85

Table 1. FENet frameworks achieve **state-of-the-art CULane** performance with efficient GFlops. FENetV1 obtains the top mF1 and F1@75 scores, surpassing all methods including optimal CLRNet, showcasing advanced lane recognition. FENetV2 closely matches V1 metrics and we recommend it more for practical use, as analyzed in subsequent sections regarding its advantages.

and necessary steering adjustments. To address this mismatch between current evaluations and necessary lane understanding for driving, we propose augmenting assessment through a Partial Field of View metric. This practical approach subdivides the lower image half into fractional views after pre-processing cropping of irrelevant upper content. As visualised in Fig. 5, by quantifying accuracy on key distal fraction views (the top 1/2 and top 1/3 fields), the metric better gauges precision for the most critical lane regions corresponding to human driver gaze. The Partial Field analysis provides a closer approximation to human perception. It constitutes an interpretable enhancement measuring lane detection aptitude through the practical lens of on-road gaze patterns.

4. EXPERIMENT

4.1. Datasets

In this experiment, we employ the most commonly used datasets in lane detection: CULane [9] and LLAMAS [23]. CULane is currently one of the most challenging large-scale datasets for lane detection. LLAMAS is a comprehensive lane detection dataset comprising over 100,000 images. Lane markings within LLAMAS are auto-annotated employing high-precision maps.

4.2. Implementation Details

Primarily, DLA34 is used as the backbone network for pre-training in this study [24]. Under the DLA34 backbone network, the CULane dataset is set to iterate for 15 epochs while LLAMAS is set to 20. The initial learning rate is set to $1e-3$, the optimizer is AdamW, and the power is set at 0.9. The number of lane priors (N) is 72, and the number of sampling points is 36. In the expansion pixels (m) for P_{IoU} , DL_{IoU} and DR_{IoU} are all set to 15. The coefficient of assigning cost is set as $\omega_{DioU} = 1$.

4.3. Evaluation Metrics

F1 and mF1. In the F1 test, the IoU is calculated between the prediction and the ground truth, and when the IoU threshold is greater than 0.5, it is considered a True Positive. The F1 is defined as:

$$F_1 = \frac{2 \times Precision \times Recall}{Precision + Recall} \quad (8)$$

About the COCO detection metric, we primarily continue to use the mF1 metric as the following metric in CLRNet, but to measure not only the overall performance but also the **scenes' performance**, providing a more precise analysis of prediction accuracy and lane feature capture. The mF1 is defined as:

$$mF_1 = (F1@50 + F1@55 + \dots + F1@95)/10 \quad (9)$$

where F1@50, F1@55, ..., F1@95 correspond to the F1 test values when the IoU threshold is 0.5, 0.55, ..., and 0.95, respectively. This is a more precise measurement in different scenes and has a significant effect on optimization iteration.

4.4. Comparison with State-of-the-Art Results

Performance on CULane. Our proposed FENet achieves state-of-the-art results on the CULane benchmark, surpassing prior methods. As shown in Table 1, FENetV1 obtains an F1@75 score of **63.63** and an mF1 of **56.27**, **exceeding** CLRNet's F1@75 by **0.7** and mF1 by **0.63**. FENetV2 obtains an F1@75 score of **63.50** and an mF1 of **56.17**, this demonstrates FENetV1's and FENetV2's precision for lane detection, particularly at stricter evaluation thresholds.

Performance by Field of View. As Table 2 shows, compared to the state-of-the-art CLRNet model, FENetV2 demonstrates significantly improved curved and distant lane detection across the entire, the top half, and the top third field of views. Importantly, in the vast majority of driving scenarios, bend characteristics are mainly reflected from afar. Thus these gains primarily represent an enhanced perception of distant curved lanes, which is critical for safe maneuvering. Specifically, as shown by data marked with *, FENetV2

Field of View	Backbone	mF1	Normal	Crowded	Dazzle	Shadow	No line	Arrow	Curve	Cross	Night
Whole View of Lane											
CLRnet	DLA34	55.64	68.72	53.81	47.4	53.24	35.28	65.56	40.62	1154	49.59
FENetV1 (Ours)	DLA34	56.27	68.7	55.12	48.16	52.77	35.32	65.57	42.11	1147	50.51
FENetV2 (Ours)	DLA34	56.17	69.19	54.38	47.67	53.39	35.15	66.03	43.29*	1206	50.55
Top 1/2 View of Lane											
CLRnet	DLA34	60.17	73.83	57.55	53.24	57.69	38.8	69.81	38.88	1155	55.3
FENetV1 (Ours)	DLA34	61.08	74.11	59.09	53.92	58.46	38.48	69.98	41.92	1147	56.69
FENetV2 (Ours)	DLA34	60.97	74.59	58.21	53.75	58.5	38.59	70.33	44.54*	1206	56.73
Top 1/3 View of Lane											
CLRnet	DLA34	58.53	72.46	55.84	52.84	53.89	38.48	67.76	31.1	1155	53.13
FENetV1 (Ours)	DLA34	59.71	73.06	57.45	53.86	55.29	38.28	67.99	34.61	1147	55.04
FENetV2 (Ours)	DLA34	59.53	73.5	56.43	54.03	54.53	38.49	68.07	37.11*	1206	55.05

Table 2. Performance by Field of View. Compared to optimal CLRNet, FENet demonstrates mF1 gains over entire, the top 1/2, and top 1/3 views. Particularly significant curved and distant lane improvements manifest, with FENetV2 curve detection higher by 2.67, 5.66, and 6.01 on those views respectively. This highlights FENetV2’s advantages on challenging curves versus prior works. Overall, FENetV2 surpasses V1 on regression precision due to its D-IOU loss and FEFPN enabling optimized boundary localization. However, FENetV1 exhibits greater competency on lane recognition itself rather than regression due to its PEFPN inferring spatial layouts effectively.

Method	Backbone	Valid		
		mF1	F1@50	F1@75
PolyLaneNet	EfficientnetB0	48.82	90.2	45.4
LaneATT	ResNet-18	69.22	94.64	82.36
LaneATT	ResNet-34	69.63	94.96	82.79
LaneATT	ResNet-122	70.8	95.17	84.01
LaneAF	DLA-34	69.31	96.9	84.71
CLRNet	DLA-34	71.21	97.16	85.33
FENetV2(Ours)	DLA-34	71.85	96.97	85.63

Table 3. FENetV2 establishes new **state-of-the-art LLAMAS** results, proving advanced lane detection aptitude. Our approach sets the top mF1 using the DLA-34 backbone while exceeding all methods on the vital long-range F1@75.

achieves **2.67, 5.66, and 6.01 higher** mF1 scores for detecting challenging far-ahead curved lanes in that respective field of views. This highlights FENetV2’s particular strengths in precisely identifying tricky distant and curved lanes, enabled by its D-IoU loss function and FEFPN module. Some supporting example results are provided in Fig. 6 in Appendix A.1.

Although FENetV1 achieves slightly higher overall mF1 scores, we argue that FENetV2 is much more suitable and reliable for real-world self-driving systems due to its specialization for distant lane boundary regression. Accurately localizing lane lines far ahead is vital for timely vehicle control reactions, especially at faster speeds. In contrast, while FENetV1’s PEFPN exhibits strengths in general lane recognition, it has limitations in precision boundary localization. In summary, FENetV2 demonstrates the best real-world lane detection competency due to its specialization in distant lane regression, unlike prior state-of-the-art models. For practical autonomous navigation requiring split-second reactions,

we strongly advocate for FENetV2 over existing methods and even the baseline FENetV1 model.

Performance on LLAMAS. As Table 3 shows, the innovative FENetV2 structure proposed in this study achieves a new technical level on LLAMAS, with an F1@75 score of **85.63** and an mF1 score of **71.85**. These major scoring parameter results are higher than those of CLRNet, with the F1@75 score being **0.3 higher** than of CLRNet and the mF1 score being **0.64 higher** than that of CLRNet. This also indicates that our method makes improvements in lane detection accuracy.

5. CONCLUSION

Inspired by human driving focus, this research pioneers Focusing on Enhanced networks, sampling strategies, optimized loss calculations, and refined evaluation metrics targeting lane detection challenges for autonomous navigation. Experiments demonstrate emphasizing critical distant geometric details, unlike existing uniform approaches, significantly improves not only benchmark accuracy but also practical curved/distant lane recognition essential for safety. Advancements derive from isolating perspective-aware contexts mimicking adept driver vision patterns. Limitations provide opportunities including refining attention regions, exploring enriched coordinate representations, collecting actual driving data for analysis, and reconciling dual frameworks exploiting complementary strengths - furthering real-world breakthroughs. With human-mimicking visual perception and comprehension as a guide, the lane detection frontier can rapidly advance toward enabling reliable autonomous vehicle control.

6. REFERENCES

- [1] Otto Lappi, Paavo Rinkkala, and Jami Pekkanen, “Systematic observation of an expert driver’s gaze strategy—an on-road case study,” *Frontiers in Psychology*, vol. 8, apr 27 2017, [Online; accessed 2023-12-28].
- [2] Esko Lehtonen, Otto Lappi, Iivo Koirikivi, and Heikki Summala, “Effect of driving experience on anticipatory look-ahead fixations in real curve driving,” *Accident Analysis & Prevention*, vol. 70, pp. 195–208, 2014.
- [3] Ronald R Maurant and Thomas H Rockwell, “Strategies of visual search by novice and experienced drivers,” *Human factors*, vol. 14, no. 4, pp. 325–335, 1972.
- [4] Erwin R Boer, “What preview elements do drivers need?,” *IFAC-PapersOnLine*, vol. 49, no. 19, pp. 102–107, 2016.
- [5] Tu Zheng, Yifei Huang, Yang Liu, Wenjian Tang, Zheng Yang, Deng Cai, and Xiaofei He, “Clrnet: Cross layer refinement network for lane detection,” in *Proceedings of the IEEE/CVF conference on computer vision and pattern recognition*, 2022, pp. 898–907.
- [6] Jinsheng Wang, Yinchao Ma, Shaofei Huang, Tianrui Hui, Fei Wang, Chen Qian, and Tianzhu Zhang, “A keypoint-based global association network for lane detection,” in *Proceedings of the IEEE/CVF Conference on Computer Vision and Pattern Recognition*, 2022, pp. 1392–1401.
- [7] Ashish Vaswani, Noam Shazeer, Niki Parmar, Jakob Uszkoreit, Llion Jones, Aidan N Gomez, L ukasz Kaiser, and Illia Polosukhin, “Attention is all you need,” in *Advances in Neural Information Processing Systems*, I. Guyon, U. Von Luxburg, S. Bengio, H. Wallach, R. Fergus, S. Vishwanathan, and R. Garnett, Eds. 2017, vol. 30, Curran Associates, Inc.
- [8] Qingquan Li, Long Chen, Ming Li, Shih-Lung Shaw, and Andreas Nüchter, “A sensor-fusion drivable-region and lane-detection system for autonomous vehicle navigation in challenging road scenarios,” *IEEE Transactions on Vehicular Technology*, vol. 63, no. 2, pp. 540–555, 2014.
- [9] Xingang Pan, Jianping Shi, Ping Luo, Xiaogang Wang, and Xiaoou Tang, “Spatial as deep: Spatial cnn for traffic scene understanding,” in *Proceedings of the AAAI Conference on Artificial Intelligence*, 2018, vol. 32.
- [10] Yuenan Hou, Zheng Ma, Chunxiao Liu, and Chen Change Loy, “Learning lightweight lane detection cnns by self attention distillation,” in *Proceedings of the IEEE/CVF international conference on computer vision*, 2019, pp. 1013–1021.
- [11] Hang Xu, Shaoju Wang, Xinyue Cai, Wei Zhang, Xiaodan Liang, and Zhenguo Li, “Curvelane-nas: Unifying lane-sensitive architecture search and adaptive point blending,” in *Computer Vision–ECCV 2020: 16th European Conference, Glasgow, UK, August 23–28, 2020, Proceedings, Part XV 16*. Springer, 2020, pp. 689–704.
- [12] Seungwoo Yoo, Hee Seok Lee, Heesoo Myeong, Sunggrack Yun, Hyoungwoo Park, Janghoon Cho, and Duck Hoon Kim, “End-to-end lane marker detection via row-wise classification,” in *Proceedings of the IEEE/CVF conference on computer vision and pattern recognition workshops*, 2020, pp. 1006–1007.
- [13] Yuenan Hou, Zheng Ma, Chunxiao Liu, Tak-Wai Hui, and Chen Change Loy, “Inter-region affinity distillation for road marking segmentation,” in *Proceedings of the IEEE/CVF Conference on Computer Vision and Pattern Recognition*, 2020, pp. 12486–12495.
- [14] Zequn Qin, Huanyu Wang, and Xi Li, “Ultra fast structure-aware deep lane detection,” in *Computer Vision–ECCV 2020: 16th European Conference, Glasgow, UK, August 23–28, 2020, Proceedings, Part XXIV 16*. Springer, 2020, pp. 276–291.
- [15] Zequn Qin, Pengyi Zhang, and Xi Li, “Ultra fast deep lane detection with hybrid anchor driven ordinal classification,” *IEEE transactions on pattern analysis and machine intelligence*, 2022.
- [16] Lizhe Liu, Xiaohao Chen, Siyu Zhu, and Ping Tan, “Conclanenet: a top-to-down lane detection framework based on conditional convolution,” in *Proceedings of the IEEE/CVF International Conference on Computer Vision*, 2021, pp. 3773–3782.
- [17] Lucas Tabelini, Rodrigo Berriel, Thiago M Paixao, Claudine Badue, Alberto F De Souza, and Thiago Oliveira-Santos, “Keep your eyes on the lane: Real-time attention-guided lane detection,” in *Proceedings of the IEEE/CVF conference on computer vision and pattern recognition*, 2021, pp. 294–302.
- [18] Zhengyang Feng, Shaohua Guo, Xin Tan, Ke Xu, Min Wang, and Lizhuang Ma, “Rethinking efficient lane detection via curve modeling,” in *Proceedings of the IEEE/CVF Conference on Computer Vision and Pattern Recognition*, 2022, pp. 17062–17070.
- [19] Leonard Rusli, Brilly Nurhalim, and Rusman Rusyadi, “Vision-based vanishing point detection of autonomous navigation of mobile robot for outdoor applications,” *Journal of Mechatronics, Electrical Power, and Vehicular Technology*, vol. 12, no. 2, pp. 117–125, 2021.
- [20] Xiaolong Wang, Ross Girshick, Abhinav Gupta, and Kaiming He, “Non-local neural networks,” in *Proceedings of the IEEE conference on computer vision and pattern recognition*, 2018, pp. 7794–7803.
- [21] Liang-Chieh Chen, George Papandreou, Florian Schroff, and Hartwig Adam, “Rethinking atrous convolution for semantic image segmentation,” *arXiv preprint arXiv:1706.05587*, 2017.
- [22] Jonathan Long, Evan Shelhamer, and Trevor Darrell, “Fully convolutional networks for semantic segmentation,” in *Proceedings of the IEEE conference on com-*

puter vision and pattern recognition, 2015, pp. 3431–3440.

- [23] Karsten Behrendt and Ryan Soussan, “Unsupervised labeled lane markers using maps,” in *Proceedings of the IEEE/CVF international conference on computer vision workshops*, 2019, pp. 0–0.
- [24] Fisher Yu, Dequan Wang, Evan Shelhamer, and Trevor Darrell, “Deep layer aggregation,” in *Proceedings of the IEEE conference on computer vision and pattern recognition*, 2018, pp. 2403–2412.

A. APPENDIX

A.1. Ablation Studies

To validate the contributions and roles of each component of the entire FENetV1 and FENetV2 model in the overall experiment, we separately test each innovative scheme on the CULane dataset to display their corresponding performance.

A.2. Overall Ablation Study

Through ablation studies, we analyse our proposed FENetV1 architecture in Appendix A.1 Table 4 to analyse the contributions of the PEFPN, Focusing Sampling, and D-IoU modules. The baseline FENetV1 achieved an mF1 of 55.64. With the addition of the PEFPN and Focusing Sampling modules, the mF1 increased to 56.27, demonstrating their benefits in providing positional-aware features and emphasising hard examples. However, surprisingly, incorporating D-IoU on top of PEFPN and Focusing Sampling resulted in a slight decrease in mF1 to 56.04. We hypothesise that this counter-intuitive result is due to some functional overlap between the position-aware capabilities of PEFPN and the directional encoding of D-IoU. Specifically, the positional non-local block within PEFPN already integrates coordinate information into the multi-scale features. Thus, the directional modelling of D-IoU becomes somewhat redundant and interferes with the positional encodings of PEFPN. This integration of position and direction within PEFPN may explain why the subsequent addition of D-IoU leads to detrimental effects due to duplicate functionality.

Further ablation experiments are conducted on the contribution of each component of our proposed FENetV2 model in Appendix Table 5. The baseline architecture achieves an mF1 of 55.64. Adding the FEFPN module improves mF1 to 56.11 by providing richer multi-scale features. Incorporating Focusing Sampling further boosts mF1 to 56.15 by emphasising hard far-end examples. Finally, replacing the IoU loss with the D-IoU loss increases mF1 to 56.17 by encoding orientation cues. The steady improvements validate the benefits of FEFPN for contextual features, Focusing Sampling for handling distant lanes, and D-IoU for differentiating directionality.

In summary, the ablation study of FENetV1 reveals that Enhanced FPN with position-aware representations through PEFPN and emphasising the complementary strengths of hard samples via Focusing Sampling improved mF1 to 56.27. However, the D-IoU conceived with the ideology of positional non-local blocks may exhibit redundancy with the positional modelling already encoded within PEFPN, culminating in a slight degradation in mF1 performance. In contrast, the stable mF1 enhancement conferred by each constituent in the FENetV2 ablation experiments verifies their efficacy in assimilating rich multi-scale features, accentuating challenging regions, and embedding directional clues within our FENetV2

framework. Despite a minor decline in mF1 compared to FENetV1, superior scene-fitting accuracy is demonstrated in the manuscript. This analysis proffers constructive perceptions into the architectural trade-offs between positional non-local blocks and D-IoU formulations.

A.3. Ablation Study of Focusing Sampling

To further analyse the efficacy of our proposed Focusing Sampling technique, we conduct ablation studies comparing models with and without Focusing Sampling in Appendix Table 6. Using uniform sampling as the baseline, the model achieved an mF1 of 55.64. Replacing this with Focusing Sampling provided a slight boost to 55.78, indicating its benefits for emphasising challenging examples. The advantages of Focusing Sampling become more pronounced when coupled with our feature-enhanced FPN modules. With uniform sampling, the FEFPN and PEFPN models obtain similar mF1 scores of 56.11. However, the addition of Focusing Sampling improves their mF1 to 56.15 and 56.27 respectively. This demonstrates that Focusing Sampling better utilises the rich lane features provided by FEFPN and PEFPN, by concentrating training on the most difficult far-end regions. Notably, FEFPN and PEFPN achieve the same mF1 without Focusing Sampling. This suggests that with uniform focus, neither FPN variant could fully leverage their learned features. However, by centralizing attention, PEFPN integrated positional information to boost performance above FEFPN. Overall, these ablation studies validate that Focusing Sampling effectively complements advanced FPN modules by enabling concentrated learning on hard examples. The gains are amplified when combined with FPN designs that encode multi-scale semantics and spatial coordinates.

PEFPN	Focusing Sampling	D-IoU	mF1	F1@50	F1@60	F1@70	F1@80	F1@90
			55.64	80.09	76.19	68.99	53.97	20.51
✓			56.11	80.04	76.32	69.32	54.71	21.46
✓	✓		56.27	80.16	76.54	69.54	55.02	21.53
✓	✓	✓	56.04	80.04	76.24	69.26	54.66	21.6

Table 4. The effects of each module in the FENetV1 method. Results based on CULane.

FEFPN	Focusing Sampling	D-IoU	mF1	F1@50	F1@60	F1@70	F1@80	F1@90
			55.64	80.09	76.19	68.99	53.97	20.51
✓			56.11	80.24	76.35	69.39	54.82	21.55
✓	✓		56.15	80.04	76.35	69.49	55.14	21.44
✓	✓	✓	56.17	80.19	76.36	69.2	54.93	21.79

Table 5. The effects of each module in the FENetV2 method. Results based on CULane.

Sampling Settings	mF1	F1@50	F1@60	F1@70	F1@80	F1@90
Uniform sampling	55.64	80.47	76.19	68.99	53.97	20.51
Uniform sampling + FEFPN	56.11	80.24	76.35	69.39	54.82	21.55
Uniform sampling + PEFPN	56.11	80.04	76.32	69.32	54.71	21.46
Focusing Sampling	55.78	79.93	76.03	68.72	54.24	21.56
Focusing Sampling + FEFPN	56.15	80.04	76.35	69.49	55.14	21.44
Focusing Sampling + PEFPN	56.27	80.16	76.54	69.54	55.02	21.53

Table 6. The ablation research for Focusing Sampling in PEFPN(FENetV1) and FEFPN(FENetV2) methods. Results based on CULane.

	Curve lane lines	Distant lane lines
Ground Truth		
CLRNet		
FENetV2 (Ours)		
	Hidden lane lines	Worn lines
Ground Truth		
CLRNet		
FENetV2 (Ours)		

Fig. 6. Comparison of the detection effect of curve, distant, hidden and worn lane lines on some difficult samples with ground truth. The upper right corner of each image results from a 4x pixel magnification of the human eye focus position for the front ahead.

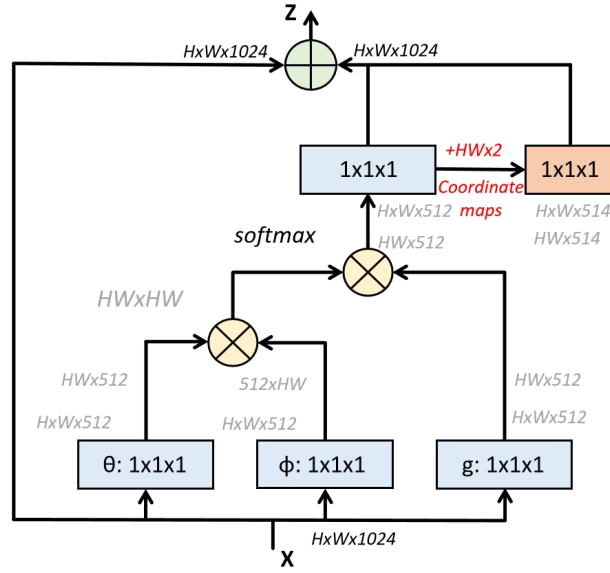


Fig. 7. Illustration of positional non-local blocks. The extra coordinate maps are fused at the rear of the original non-local block.

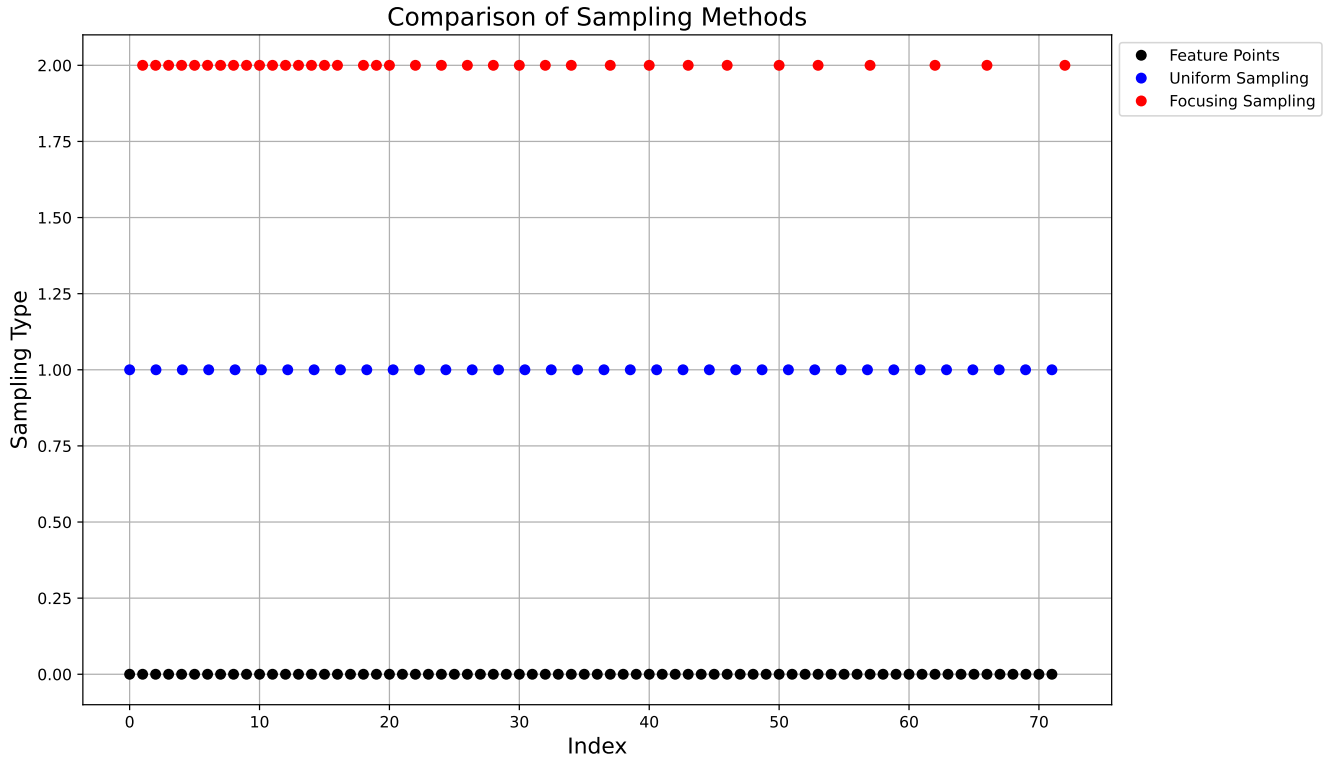


Fig. 8. Focusing Sampling and uniform sampling intuitive comparison. The black dots in the figure denote 72 feature points. The blue dots signify feature points selected via uniform sampling, while the red dots mark feature points chosen through Focusing Sampling. The feature point Focusing Sampling in this work proceeds from densely populated feature point regions in distant areas of the visual scene, progressing toward more sparsely distributed features in proximity to the observer.